CHEMISTRY OF MATERIALS

pubs.acs.org/cm Article

Scalable Gas-Phase Purification of Boron Nitride Nanotubes by Selective Chlorine Etching

Hyunjin Cho, Steven Walker, Mark Plunkett, Dean Ruth, Robyn Iannitto, Yadienka Martinez Rubi, Keun Su Kim, Christa M. Homenick, Andreas Brinkmann, Martin Couillard, Stéphane Dénommée, Jingwen Guan, Michael B. Jakubinek, Zygmunt J. Jakubek, Christopher T. Kingston, and Benoit Simard*

Cite This: *Chem. Mater.* 2020, 32, 3911−3921 Read Online

ACCESS | Metrics & More | Article Recommendations | Supporting Information

ABSTRACT: Current processes to manufacture nanotubes at commercial scales are unfortunately imperfect and commonly generate undesirable byproducts. After manufacturing, purification is necessary and is a rate and cost determining step in advancing the development of commercial products based on nanotubes. Boron nitride nanotubes (BNNTs) produced without metal catalysts from high-temperature processes are known to contain a significant amount (e.g., 50 wt %) of various boron derivatives. Herein we report a simple yet efficient and scalable process to purify these types of BNNT materials at commercial scales, from a few grams to hundreds of grams, at purity over 85 wt % in a single step. The process relies on a vertically mounted flow tube reactor and scrubber system that can be operated under pure or diluted chlorine gas flow at temperatures up to 1100 °C. The main chemical reactions driving the purification are the conversion of boron and BN derivatives into BCl_3 and HCl, which are removed as gaseous species, while pristine BNNTs are left behind. The preferential etching of impurities over pristine BNNTs shows the extreme chemical resistance of BNNTs in this harsh environment and opens up new applications for this nanomaterial. The process has been examined at various temperatures, up to 1050 °C, and the resulting materials display improved BNNT purity and quality across a range of imaging and spectroscopic assessments. The recommended temperature to optimize quality with yield is 950 °C, although higher quality material is obtained at a higher temperature.

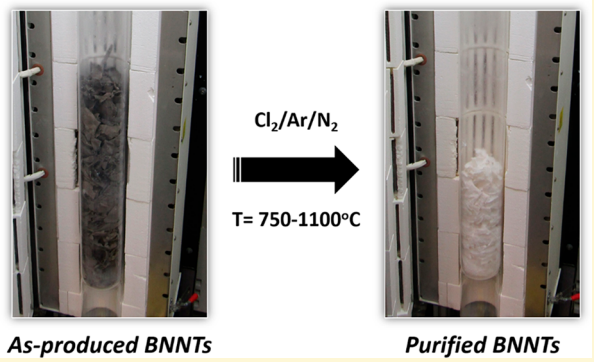

INTRODUCTION

Boron nitride nanotubes (BNNTs) are one-dimensional nanomaterials structurally analogous to carbon nanotubes (CNTs) and possess equally impressive mechanical properties along with a different set of multifunctional features including higher thermal stability, electrical insulation, high neutron absorption, and transparency in the visible region.[1−11] Advances in large-scale BNNT production are now enabling broader availability of BNNT materials for research and applications[11−15] and have resulted in some recently available commercial supplies.[16−20] From a commercial perspective, high-temperature manufacturing methods exhibit great promise. These methods do not require the use of metal catalysts, and they employ simple feedstocks (e.g., elementary boron or hexagonal boron nitride, h-BN) and simple gases (e.g., nitrogen, argon, and hydrogen).[16−20] In these processes, the feedstocks are thermally vaporized to produce appropriate precursor species that subsequently condense to a critical density for BNNT nucleation and growth.[17,18] The BNNTs produced by these methods are highly crystalline, possess few walls (generally fewer than 10), and have aspect ratios (length/diameter) greater than 500; however, the materials contain many impurities. The impurities, which can exceed 50−60 wt % in some cases, include allotropes of boron, various saturated and unsaturated boron-containing polymers, and amorphous and crystalline boron nitride compounds. Removing these impurities is essential to extract the full potential of BNNTs in various applications.

Several purification methods have been reported to date[21−25] which can be generally classified into four groups: liquid-phase treatments, gas-phase treatments, combinations thereof, and solid−liquid phase treatments. Liquid-phase treatments include acid oxidation,[21] bromine treatment,[22] superacid extraction,[23] and hydrocarbon extraction.[24] The drawbacks of these methods include limited effectiveness, damage to the BNNTs, limited scalability, high cost, significant environmental footprint, and extensive densification of BNNTs

Received: January 13, 2020
Revised: April 9, 2020
Published: April 9, 2020

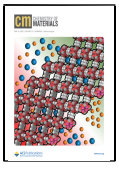

https://dx.doi.org/10.1021/acs.chemmater.0c00144
Chem. Mater. 2020, 32, 3911−3921

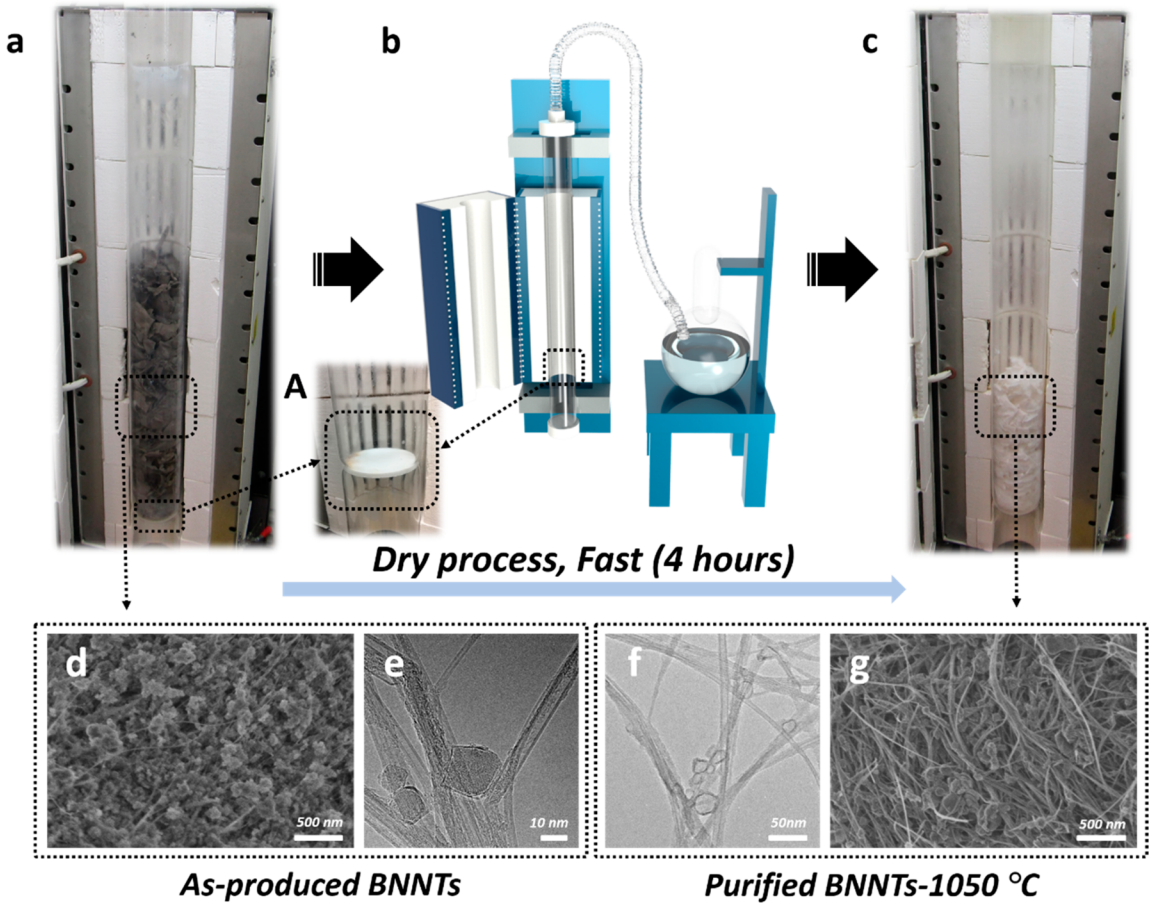

Figure 1. Purification process up to 150 g scale. (a) Photograph of ap-BNNTs prior to purification (inset A shows a coarse frit disk in the quartz tube). (b) Schematic of the purification process of BNNTs. (c) Photograph of purified BNNTs. (d) SEM image of the ap-BNNTs. (e) TEM image of the ap-BNNTs. (f) TEM image of the purified BNNTs. (g) SEM image of the purified BNNTs.

when the solvent is removed. The latter makes it difficult to redisperse the BNNT in solvents or matrices. The main advantage of these methods is that they are carried out at or near room temperature in widely accessible laboratory glassware. Gas-phase treatments include water vapor treatments at high temperatures (>700 °C).[25] In this purification approach water serves as an oxygen source to transform elemental boron or terminated B edges into borates and as a hydrogen source to transform borates into hydrogen borates, which are sublimated at temperatures above 600 °C. The main drawbacks of this method are that it is time-consuming due to low transformation rates and that it offers very low yields (<10%) due to chemical etching of BNNTs. The main advantages of this method, however, are good scalability, low processing cost, and minimal environmental footprint due to the fact that the method is gas-phase entirely and the reagents are water and oxygen. Combinations of gas and liquid-phase treatments include air oxidation at elevated temperatures.[17,26] In that case, the first step, gas-phase oxidation using molecular oxygen as a reagent to transform elementary boron and terminated boron edges into boron oxides (B_2O_3), is followed by a liquid phase step, usually in water or methanol, to remove the created boron oxides. The approach removes boron oxides quite effectively, but it is not efficient for terminated boron edges or other types of impurities. The main drawbacks of this method are that the temperature for air oxidation (>600 °C) is also the temperature at which other reactions with the BNNTs occur. Additionally, boron oxide is created in the liquid state and wets materials with a protective layer against further oxidation. This boron oxide coating is hard to remove by solution-phase treatments without solubilizing the BNNTs because the boron oxide acts as a surfactant. A solid−liquid phase treatment has been reported in which a liquid or near liquid state ferric chloride salt at temperatures generally between 250 and 350 °C is used to penetrate and wet the internal surfaces of BNNTs to dissolve impurities.[27] For the process to work effectively, conditions that cause the salt to decompose must be avoided. Other reagents such as HCl at room temperature and heating in air to 700 °C can be used to remove impurities that cannot be dissolved using the molten salt alone. The main drawbacks of this method are its limited scalability, use of corrosive molten metallic salts, multistep washing cycles, and significant environmental footprint. Typical yields from this method are not reported; however, given the multistep washing cycles, the yields are presumably low. As such, while there are a number of recent advances in BNNT purification, current routes to purify BNNTs have many deficiencies, and these must be resolved to fully exploit the commercial potential of BNNTs.

Herein we report a simple process that resolves many of the issues listed above. The key features of the process are scalability (up to 150 g batches demonstrated), low carbon footprint (gas-phase process with byproducts entirely soluble in water), and high yield (approximately 30−70 wt %

https://dx.doi.org/10.1021/acs.chemmater.0c00144
Chem. Mater. 2020, 32, 3911−3921

depending on the temperature). The overall cost of the method also represents only a small fraction of the production cost of BNNTs, which is critical to achieving industrially viable BNNT manufacturing. To illustrate the effectiveness of the process, all of the BNNT materials were evaluated using a battery of characterization methods, including thermogravimetric analysis coupled with Fourier transform infrared (TGA-FTIR) spectroscopy, FTIR spectroscopy, UV−vis absorption spectroscopy, X-ray photoelectron spectroscopy (XPS), solid-state nuclear magnetic resonance (NMR) spectroscopy, field emission scanning electron microscopy (FE-SEM), transmission electron microscopy (TEM), scanning transmission electron microscopy (STEM), energy-dispersive X-ray spectroscopy (EDS), and electron energy loss spectroscopy (EELS). The enhancement in the quality of the BNNT material was also confirmed using our recently reported titration method with regiorandom-poly(3-hexyl-thiophene) (rra-P3HT).[28,29]

CHEMICAL BASIS OF THE PROCESS

The process presented here is applicable to all as-produced BNNT (ap-BNNT) materials produced using high-temperature processes. One such process is the hydrogen-assisted BNNT synthesis (HABS) process,[17,18] and the material used in this paper was produced using the HABS method. This ap-BNNT material consists of approximately 50 wt % BNNTs with impurities of about 25 wt % boron allotropes and 25 wt % BN, which includes polymer derivatives with the generic composition $B_xN_yH_z$. The basic chemical reactions underlying the purification process are in order of importance

$$2B(s) + 3Cl_2(g) \rightarrow 2BCl_3(g) \quad (1)$$

$$2BN(s) + 3Cl_2(g) \rightleftharpoons 2BCl_3(g) + N_2(g) \quad (2)$$

$$B_xN_yH_z(s) + Cl_2(g) \rightarrow BN(s) + HCl(g) \quad (3)$$

$$B_wN_xO_yH_z(s) + Cl_2(g) \rightarrow BN(s) + ClO_p(g) + HCl(g) \quad (4)$$

The BN produced in the minor reactions 3 and 4 is fed into the equilibrium reaction 2; therefore, the final reaction products are all gaseous species and are removed from the reactor by the constant gas flow (*vide infra*). Reaction 1 has an onset at about 425 °C. The dehydrogenation of the $B_xN_yH_z(s)$ derivatives in reaction 3 and removal of oxides in reaction 4 occur over an extended temperature range from 300 to 900 °C.[30] As the reaction products are constantly vented from the reactor, the equilibrium in reaction 2 is shifted to the right toward the formation of gaseous byproducts. Bartl et al. used reaction 2 to selectively etch h-BN over c-BN in the CVD growth of diamond and c-BN.[31] The onset of this reaction was over 700 °C. Since BNNTs share the same hexagonal bonding network as h-BN, one could expect BNNTs to react similarly, and indeed structurally defective BNNTs do react in the same fashion. The h-BN present in the ap-BNNT material has unsaturated edges that are more reactive than pristine BNNTs. As will be demonstrated below, this side reaction is an unexpected positive finding of this work as it provides a way to selectively remove both impurities and defective BNNTs.

EXPERIMENTAL SECTIONS

Reactor Design. The purification system (Figure 1) consists of a 10 cm diameter 3-stage vertical oven fitted with a quartz tube. As-produced BNNTs are loaded into the quartz tube and are supported by a coarse frit disk that is secured in the quartz tube at the inlet end of the furnace (see Figure 1, inset A); the frit supports the BNNTs without inhibiting gas flow. The system is equipped with mass flow controllers to regulate the flow of Cl_2, Ar, and N_2 gases to the inlet port of the reactor. The gases flow upward through the ap-BNNT material and are vented through the top of the reactor; the resulting gaseous byproducts, from reactions 1 to 4, vent through the top of the reactor and are subsequently neutralized through a caustic NaOH solution circulating in a scrubber system. The final products in the scrubber after neutralization are mainly boric acid and sodium chloride with a small fraction of chlorite salts, which are benign compounds. A photograph of the entire apparatus is shown in Figure S1 of the Supporting Information.

Purification Procedure. The ap-BNNTs were first dried in a box furnace at 150 °C for 3 h to remove adsorbed moisture, which allows for the accurate determination of sample mass. Next, the ap-BNNTs were placed in the quartz tube and preheated to 105 °C with 300 sccm of Ar, and the reactor was sealed. The gas composition was then adjusted to a mixture of 1000 sccm of N_2 as buffer gas and 50 sccm of Ar at 105 °C and was flowed through the sample for 20 min, followed by 1000 sccm of flowing Ar at 300 °C maintained for a minimum of 3 min per gram. At this point, the temperature was increased to the target operating value for each experiment (750 °C to 1050 °C). Once the operating temperature was reached, 1000 sccm of Cl_2 and 50 sccm of Ar gas flowed through the BNNTs. A typical exposure time to completely remove boron allotropes was 3 min per gram of ap-BNNTs. After completing the purification, the flow of Cl_2 was stopped. Then, the reactor was purged for 15 min using 500 sccm of N_2 and 500 sccm of Ar prior to cooling the reactor to room temperature under the same gas flow conditions.

BNNT Production. The ap-BNNTs were prepared by the previously reported HABS method.[17,18] Briefly, h-BN powder was vaporized using an induction plasma torch operated with Ar, N_2, and H_2 gases, and the subsequent reaction conditions were controlled to favor the nucleation and growth of small-diameter and few-walled BNNTs. The ap-BNNTs were collected directly from the collection chamber without any additional treatment process.

Characterization of the BNNTs. The morphology and the surface of the ap-BNNTs and the purified BNNTs were characterized with FE-SEM (Hitachi, S4700) and TEM (FEI, Titan). For TEM analyses including STEM, EDS, and EELS, the BNNTs were sonicated in methanol using a sonication bath for 5 min followed by drop-casting onto a lacey-carbon film supported on a mesh copper grid and drying in air. TEM imaging was conducted at 300 keV. Tandem TGA-FTIR data were obtained in dry air up to 950 °C with a ramp rate of 10 °C per minute using a Netzsch STG 449 F1 TGA instrument coupled to a Bruker Tensor 27 FTIR spectrometer. ^{11}B NMR spectra were obtained at an ^{11}B Larmor frequency of 160.5 MHz in a static magnetic field of 11.75 T using a Bruker Advance-III console and a Varian 4 mm double-resonance standard-bore magic-angle spinning (MAS) probehead. The samples were rotated at a spinning frequency of 12 kHz, and a single pulse with rf field strength of 100 kHz and duration of 2.1 μs was applied prior to signal acquisition. Surface elemental analyses were carried out using dry BNNTs deposited on copper tape using a Kratos AXIS Ultra DLD XPS spectrometer and following the measurement conditions and fitting procedures we recently described for XPS assessment of similar BNNT samples.[32]

FTIR analyses of dry BNNT samples were carried out using an Agilent 630 FTIR instrument operated in attenuated total reflection (ATR) mode. All samples (each 5.0 ± 0.01 mg) for the rra-P3HT quality test were prepared and analyzed according to the method reported by Martinez-Rubi et al.[28,29] The content of BN impurities was also determined using gravimetric analyses strictly adhering to the following protocol. A total of 2 g of BNNT material was placed in a one liter bottle, and 1 L of boiling deionized water was added. The bottle was placed in a sonication bath for 15 min and subsequently filtered through a 20 μm stainless steel mesh. The filtrand was returned to the one liter bottle, and this sonication/filtration process

https://dx.doi.org/10.1021/acs.chemmater.0c00144
Chem. Mater. 2020, 32, 3911−3921

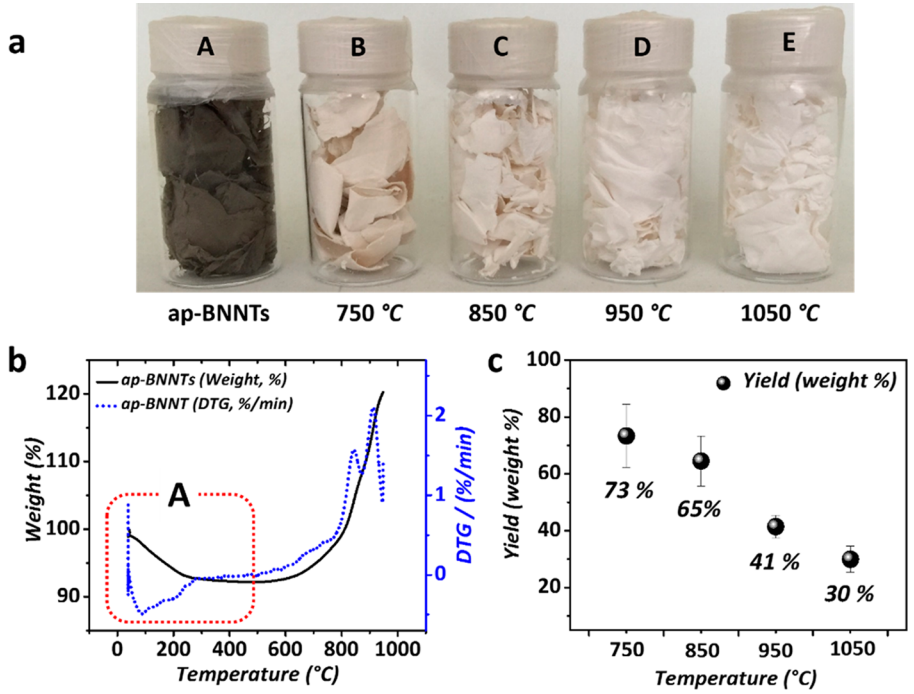

Figure 2. Comparison data between ap-BNNTs and purified BNNTs. (a) Photographic image of BNNTs purified at various temperatures. (b) TGA result for ap-BNNTs (inset A shows the mass loss). (c) Purification yield at 750 °C, 850 °C, 950 °C, and 1050 °C.

was repeated four times. After the fourth iteration the solution remained transparent after sonication. The filtrand was then dried, weighed, and the weight was compared to the initial mass of the material. The mass loss provides a good estimate for the amount of BN impurities present in the starting material.

RESULTS AND DISCUSSION

Photographs of the as-produced and purified BNNTs at 750 °C, 850 °C, 950 °C, and 1050 °C, respectively, are shown in Figure 2a. The ap-BNNTs appear as a dark brown material because of the presence of about 25 wt % of boron allotropes (elemental boron), which are byproducts of the synthesis process, as shown Figure S2a, Figure S3, and Figure S4. Figure 2b shows TGA carried out in an air atmosphere for the ap-BNNT material. Of note is the mass loss observed in the 25−300 °C temperature range (inset A of Figure 2b), which is typical of the ap-BNNT material and attributed to adsorbed water and ammonia. Water adsorption by BNNTs arises from handling in ambient atmosphere and is highly dependent on the local humidity. Ammonia is a byproduct of the synthesis as discussed in our previous paper.[17] To avoid side reactions with chlorine these species were desorbed by subjecting the as-produced material to an Ar flow at 300 °C prior to initiating purification with chlorine. Elemental boron allotropes are known to react with chlorine gas according to reaction 1. We have established the onset of this reaction at about 450 °C. At 750 °C, all of the free boron allotropes are removed, but the material appears slightly beige in color. This result is attributed to small amounts of the remaining boron allotropes encapsulated in BN shells. Complete removal of this encapsulated boron is only achieved after subjecting the BNNTs to purification at 950 °C, as evidenced by the resultant bright white appearance (Figure 2a). The SEM and TEM images in Figure 1 show the effect of chlorine exposure on the ap-BNNT material. It is clear from the presence of empty BN shells (Figure 1f, Figure S5, and Figure S6) that chlorine is capable of penetrating the BN layers to remove the encapsulated boron. Figure 2c shows a plot of the reaction yield as a function of temperature, where yield is expressed as the ratio of mass remaining in the reactor after the purification process over the initial mass of ap-BNNTs. These yields have been determined over several experiments using initial masses of ap-BNNTs of 20 to 150 g per experiment. At 750 °C, the yield is 73%. The mass loss of 27% is attributed to the removal of elemental boron according to reaction 1 and the onset of reactions 2, 3, and 4. An elemental boron content of 22% in ap-BNNTs was determined by a bromine titration (see the SI for procedure). At 850 °C, the yield drops a further 8% to 65%. Of this additional 8%, encapsulated boron accounts for a few percent at most. We attribute the majority of the additional mass loss to reactions 2, 3, and 4: the dehydrogenation of polyborazylene derivatives, the transformation of BNOH derivatives, and the etching of amorphous and hexagonal BN, respectively. At 950 °C, the yield significantly drops by an additional 24% to 41%. We attribute this mass loss to a rapid and effective etching of BN according to reaction 2 and to the etching of defective BNNTs. At 1050 °C, the yield drops by an additional 11% to 30%. This minimal mass loss shows the amazing resilience of high-quality BNNTs to harsh environments like chlorine gas at ∼1000 °C. As shown in the SEM images of Figure S2, we found that BNNTs are very stable in harsh environments, and most of the boron-containing polymers and amorphous BN compounds were gradually eliminated when the purification temperature was increased. This analysis is corroborated with the BN content at each purification temperature as determined by gravimetric analyses (Table 1). The constant BN impurity content at 950 and 1050 °C is a result of a more aggressive etching at 1050 °C which produces smaller BN particles, including smaller BNNT fragments which pass through the 50 μm-opening mesh used for the analyses.

https://dx.doi.org/10.1021/acs.chemmater.0c00144
Chem. Mater. 2020, 32, 3911−3921

Table 1. BN Impurity Content from Gravimetric Analyses for Chlorine Purified BNNT Samples at Different Temperatures

sample/temperature (°C)	BN content (wt %)
750	46
850	28
950	16
1050	16

To validate our purification mechanism further we have conducted a series of imaging and spectroscopic characterizations. TGA was used to evaluate how reaction time and temperature impacted the purification (Figure 3). Figure 3a,b displays the TGA analyses of purified BNNT samples obtained by subjecting 20 g of samples of ap-BNNTs to a constant 90 min purification time at the four different reaction temperatures. Figure 3a shows that the mass loss up to 500 °C is gradually reduced with increasing purification temperature and that there is little difference between 950 and 1050 °C purifications. Figure 3b shows the differential thermograms, which illustrate discrete mass loss events. The main event occurs at or near 100 °C, and the IR spectroscopic signature of the released material is that of water. Hence, the purified material becomes less hygroscopic as the purification temperature is increased. Water adsorption is attributed to defect sites on BN materials, including BNNTs, and/or to the presence of dangling functionalities. This data supports the hypothesis that these adsorption sites are removed as the purification temperature was increased. The effect on the purification of varying the reaction time from 30 to 180 min in 30 min increments at the fixed temperature of 1050 °C was also evaluated. Figure 3c,d shows that total TGA mass loss decreases rapidly from the sample purified for 30 min to the 60 min sample and reaches a plateau with the 90 min sample. Again, the mass loss is due to desorption of water as shown by the temperature of onset and the spectroscopic signature of water in the IR spectrum. There is a mass gain above 900 °C in the TGA for purification reaction times below 60 min, but it is absent above 90 min. We attribute this mass increase to the oxidation of materials with dangling bonds or defective sites. For treatments above 90 min, defective materials are etched away by chlorine leaving behind materials with reduced defect densities.

^{11}B NMR is a useful technique for comparing BNNT materials purified by different methods as it is sensitive to changes in boron environments. ^{11}B NMR was used to evaluate the BNNT material purified at the four different temperatures. ^{11}B is a quadrupolar nucleus with half-integer spin $I = 3/2$, resulting in a strong anisotropic quadrupolar interaction with the electric field gradient in the surrounding electron distribution. Narrowing of the NMR spectral resonance lines can be achieved by magic-angle spinning (MAS), the rapid rotation of the sample around an axis enclosing an angle of 54.74° (magic-angle) with the external static magnetic field. The resulting spectral resonances show the typical second order line shape of half-integer quadrupolar nuclei.[33] The ^{11}B NMR spectrum for the ap-BNNTs is shown in Figure 4a. The spectrum of BNNTs shows a large main peak at 10−30 ppm, which is consistent with a 3-coordinate boron atom such as found in h-BN and BNNTs.[34,35] The quadrupole couplings are nominally the same at 2.95 MHz for h-BN and 2.99 MHz for BNNTs with $\eta_Q = 0$, which are also consistent with the previous literature.[35,36] Where these materials differ is with respect to the line shape, more specifically the size of the foot, the additional peak at 1 ppm for BNNTs, and the increased baseline for the ap-BNNT sample. Polycrystalline boron is known to give a very broad signal around 0 ppm.[37]

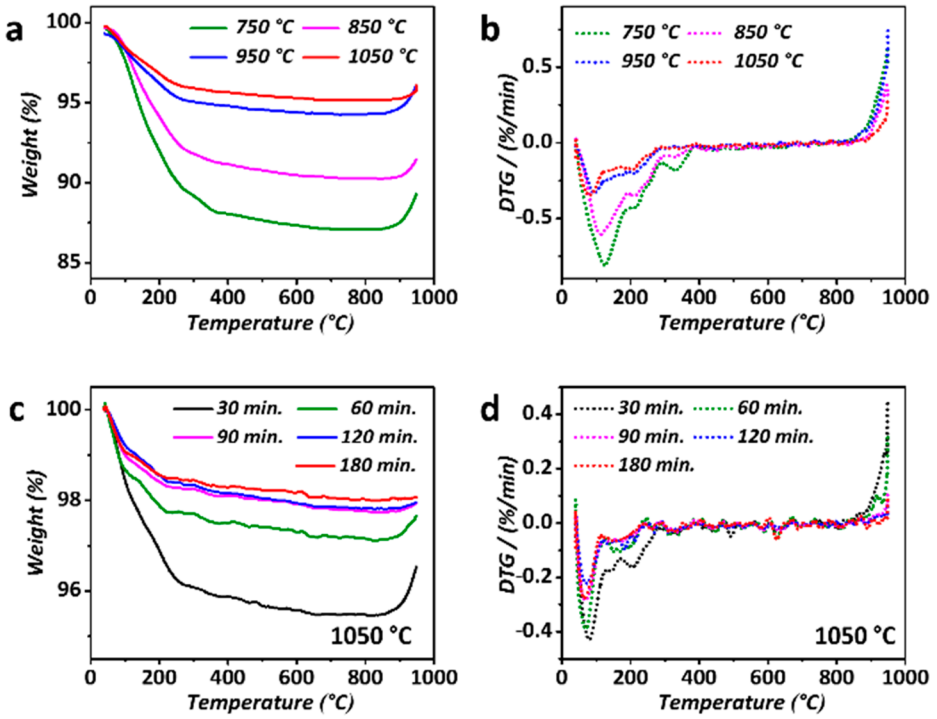

Figure 3. TGA data for purified BNNTs. (a and b) Purified at 750 °C, 850 °C, 950 °C, and 1050 °C for an initial mass of 20 g of ap-BNNT and a treatment time of 90 min. (c and d) Purified at 1050 °C for different purification times for an initial mass of 20 g of ap-BNNTs.

https://dx.doi.org/10.1021/acs.chemmater.0c00144
Chem. Mater. 2020, 32, 3911−3921

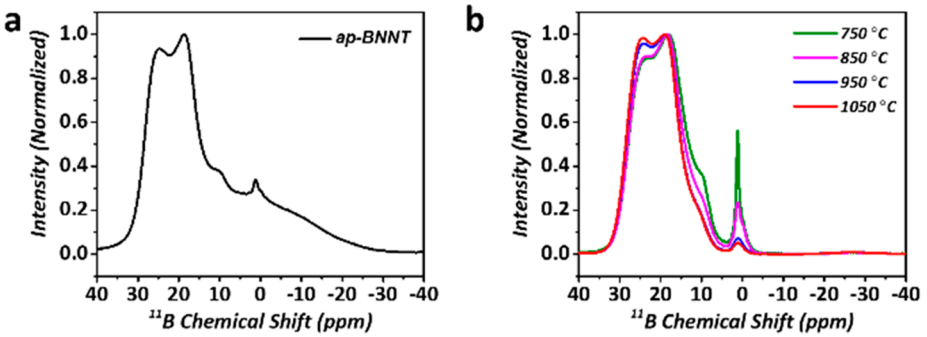

Figure 4. Solid state ^{11}B NMR data. (a) Solid state ^{11}B NMR spectrum of ap-BNNTs. (b) Solid state ^{11}B NMR spectra for BNNTs purified at 750 °C, 850 °C, 950 °C, and 1050 °C.

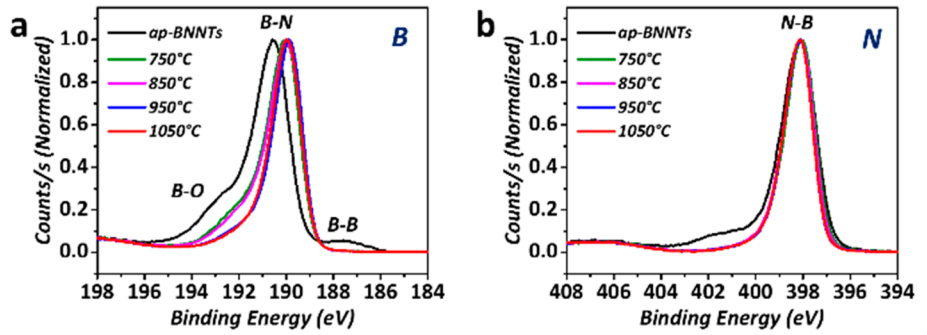

c

Sample	Survey scan					B 1s component fitting					
	Atomic composition (%)				B:N Ratio	BN		BO		BB	
	B	N	O	C		Area (%)	FWHM (eV)	Area (%)	FWHM (eV)	Area (%)	FWHM (eV)
Raw-BNNTs	45.7	35.8	14.6	3.9	1.27	70	1.40	24	2.55	6	2.29
+ Cl_2, 750 °C	47.7	37.3	11.7	3.3	1.28	82	1.37	18	2.01	-	-
+ Cl_2, 850 °C	47.7	38.0	11.1	3.2	1.25	81	1.33	19	2.07	-	-
+ Cl_2, 950 °C	49.3	41.4	6.8	2.4	1.19	88	1.24	12	1.97	-	-
+ Cl_2, 1050 °C	49.3	43.0	5.2	2.5	1.15	91	1.26	9	1.86	-	-

Figure 5. High-resolution XPS spectra of BNNTs purified at various temperatures and surface elemental composition for ap-BNNTs and purified BNNT samples. (a) XPS spectra showing the B 1s region (198−184 eV). (b) XPS spectra showing the N 1s region (408−394 eV). (c) Surface elemental composition for ap-BNNTs and purified BNNT samples, derived from XPS survey spectra, and component fitting results for the B 1s region. (The corresponding high-resolution spectra and fitting are shown in Figure S7.)

Furthermore, using ^{11}B NMR three-coordinate oxidized boron species such as BO_3 have been observed as impurities in commercial h-BN and BNNT in the foot region of the spectra.[35] Amorphous boron allotropes, BO_3, BO_4, and BN_4 environments within the ap-BNNT sample, are responsible for increasing the baseline giving the appearance of a broad monotonic underlying structure.[35] As shown in Figure 4b, upon purification even at our lowest purification temperature of 750 °C, that structure is significantly reduced if not eliminated, in close correlation with the removal of elementary boron at 750 °C. The foot, or the shoulder at 15 ppm, has been suggested[38,39] to result from rhombohedral BNNTs (r-BNNTs). However, the line shape observed at 10−30 ppm is the classic line shape of an $I = 3/2$ nucleus and can be explained by the quadrupole coupling as opposed to the presence of r-BNNTs. The more prominent appearance of the foot/shoulder in the BNNT samples speaks to the difference in the boron environment relative to h-BN, specifically the larger paramagnetic defects from either the curvature of the BNNTs relative to planar h-BN, defects in the lattice, or 3-coordinate boron oxide type impurities. The peak at 1 ppm is consistent with a 4-coordinate B−O impurity.[40,41]

As shown in Figure 4b, there are profound differences in the spectra obtained with material purified at increasing temperatures. Similar to previous BNNT materials, the quadrupole couplings are nominally the same at 2.99 MHz with $\eta_Q = 0$ for each of the samples. As the purification conditions become more aggressive, from 750 to 1050 °C, there is a narrowing of the large central peak and a reduction in the foot suggesting that the BNNT material is becoming more uniform and/or has fewer defects within the lattice, which is consistent with our proposed reaction mechanism. Furthermore, as the temperature increases there is a clear decrease in the peak at 1 ppm suggesting that the 4-coordinate B−O type impurity is being removed and the material is becoming purer. It is important to note that there is a significant decrease in the B−O type

https://dx.doi.org/10.1021/acs.chemmater.0c00144
Chem. Mater. 2020, 32, 3911−3921

impurity when the purification is performed at 950 °C but minimal additional improvement when conducted above 950 °C, which is consistent with our observation of rapid etching between 850 and 950 °C discussed earlier.

The elemental compositions of the BNNT materials as determined from XPS spectra (see Figure S7) are shown in Figure 5a–c. As we previously reported for similar BNNT materials,[32] these ap-BNNTs show a significant excess of B in compositional analysis via XPS (B:N ∼ 1.3 in this case). High-resolution spectra of the B 1s region (Figure 5a) show that the peak associated with elementary boron (near 188 eV) disappears at the lowest temperature treatment of 750 °C, suggesting that all free boron allotropes have been eliminated and in agreement with the ^{11}B NMR data and TGA analyses. Despite the absence of the elemental boron peak after purification at the lowest temperature of 750 °C, it is the higher-temperature purifications (950 and 1050 °C) that led to significant improvement in the B:N ratio. The relatively broad shoulder associated with the presence of B–O in the vicinity of ∼192 eV decreased with increasing temperature (see Figure 5a and Figure S7b–f) and is in good agreement with the ^{11}B NMR data. Fitting the component peaks in the B 1s region (Figure 5c) clearly shows that the boron environment becomes progressively more BN-like with increasing purification temperature. In order to obtain consistent fitting results, the position of the B–O component peak for the purified BNNT samples, where it becomes less pronounced, was constrained based on its position relative to the B–N peak for the ap-BNNT sample. These changes in the XPS spectra show that the more aggressive purification conditions remove further impurities, beyond removing elemental boron, and that chlorine eliminates impurities selectively at various experimental conditions, again consistent with the ^{11}B NMR data and proposed mechanism.

The oxygen content (Figure 5a and Figure S7b–f) is approximately 15% for the ap-BNNTs but decreases to 5% for BNNTs purified at 1050 °C. It is anticipated that all oxygen content can be removed if the treatment at 1050 °C is maintained for a longer time. The high oxygen content in the ap-BNNT material is surprising considering that the synthesis is carried out in a leak-free reactor. We previously reported that the oxygen content in the h-BN feedstock as determined by XPS can be as high a 7%, which is much higher than the supplier's specifications (<0.5%), and that ap-BNNTs from the HABS method showed 2% to 13% oxygen content.[32] As XPS is surface sensitive, such results likely overestimate the oxygen content of the bulk sample. It is hypothesized that oxygen present in the sample is the result of reactions between air and/or moisture with reactive species created during the BNNT synthesis when the reactor is opened to the atmosphere to collect the ap-BNNT material. Figure 5b shows the N 1s region, where only a single peak associated with B–N bonding is observed. The single peak in the N 1s region together with the B 1s peak due to B–N bonding at ∼190 eV demonstrates that the structure between boron and nitrogen is strongly maintained during the purification with Cl_2. Additionally, there is no indication of chlorine, which would have appeared in the binding energy regions of 1306 eV (for Cl LLM) and 270 eV (for Cl 2s). The Cl 2p peak overlaps with the boron region, so absorption in this region is not indicative of Cl. This is corroborated with TEM and EDS analyses presented below. The lack of any Cl functionality on the BNNT surface is expected because such a functionality would hydrolyze, readily creating B–O functionalities when the material is exposed to ambient atmosphere. However, XPS and FTIR (discussed below) data indicate that B–O functionalities decrease with increasing purification temperature. Thus, if chlorine functionalization takes place, it must be at a very low level showing the extraordinary chemical resistance of BNNTs to highly oxidative environments.

Recently, Harrison et al.[42] reported that FTIR could be a useful quantitative tool to analyze h-BN content in BNNT samples. In particular, they showed that the intensity ratio of the band near 820 cm^{-1} (out-of-plane buckling; R mode) over the in-plane bands peaking near 1350 cm^{-1} (transverse optical and longitudinal; TO modes) is a parameter sensitive to the presence of h-BN in the BNNT samples. To establish their calibration curve, Harrison et al., "spiked" their BNNT samples with well-defined quantities of h-BN powder from a single commercial source. The lower the R/TO ratio the more BNNTs within the sample. Figure S8 shows typical FTIR spectra and the R/TO ratios for 157 different BNNT measurements, including ap-BNNTs and purified BNNT samples at different temperatures. The results are independent of the casting method to prepare the samples; either dry BNNT sheets or dispersions in solvent lead to the same results. In this case, the R/TO ratios are the same within experimental error. According to Harrison et al., this would suggest that h-BN content remains the same whether the material is ap-BNNTs or purified at different temperatures. This conclusion is at odds with the data of Table 1 and with all other measurements presented in this paper. This result suggests that the FTIR method cannot be used to quantify BN impurities in BNNT material produced using the HABS process. It is feasible that the impurities present in the samples tested here differ sufficiently in structure and composition that they are not well represented by FTIR absorption at 820 cm^{-1}.

TEM analyses have also been used to examine the etching process. Figures 6 and S6 display TEM images of BNNTs

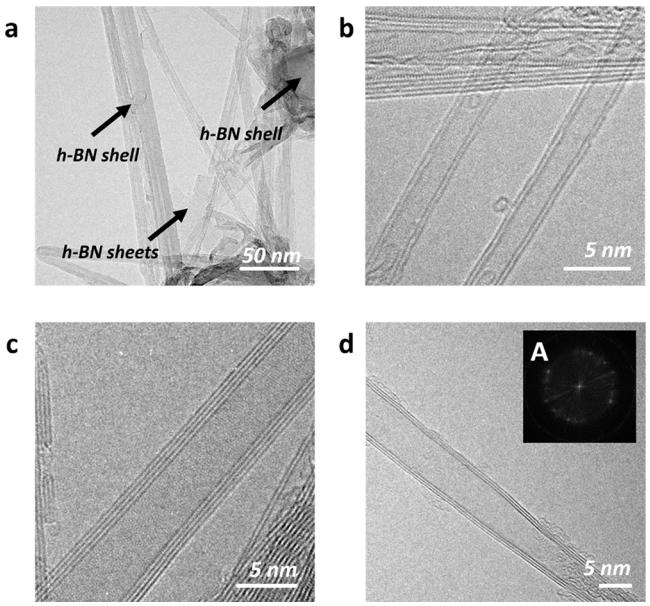

Figure 6. TEM images of the BNNTs purified at 1050 °C. (a) TEM images of BNNTs at low magnification. (b–d) TEM images of BNNTs at high magnification. (inset A of (d)) Fast Fourier transform (FFT) image of the sample.

https://dx.doi.org/10.1021/acs.chemmater.0c00144
Chem. Mater. 2020, 32, 3911–3921

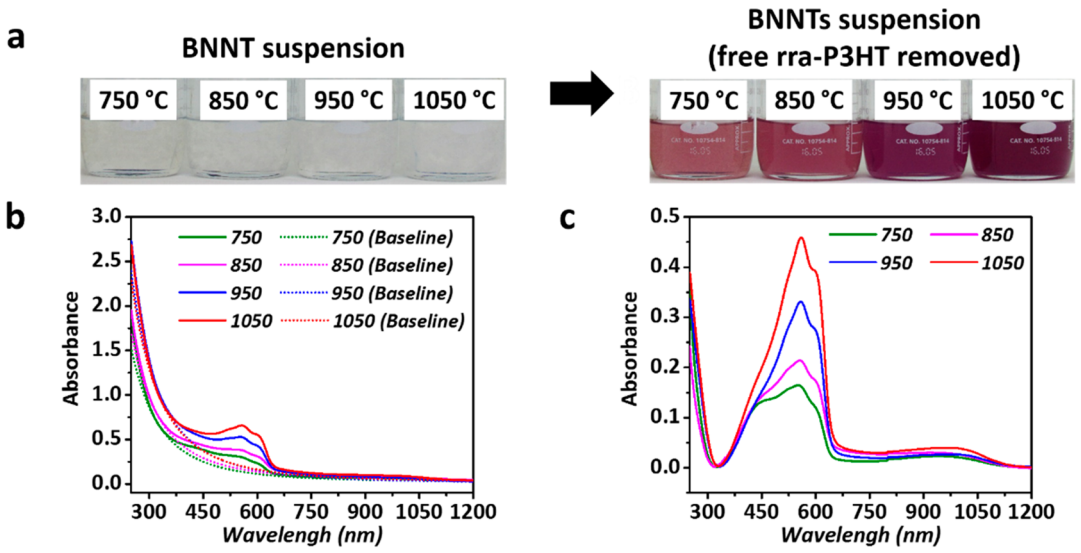

d

Purified Temperature (°C)	rra-P3HT to BNNTs mass ratio	S_{BET} (average, m^2/g)	rra-P3HT quality index $[Q_i = I(A_{1\text{-}0}) / I_{420}]$
750	0.04 < S < 0.06	117.70	1.50
850	0.06 < S < 0.08	147.05	1.87
950	0.08 < S < 0.10	184.80	2.96
1050	0.10 < S < 0.14	196.35	3.14

Figure 7. Quality assessment of BNNT using rra-P3HT. (a) Photographs of the purified BNNT (at 750 to 1050 °C) suspension in $CHCl_3$ before and after adding rra-P3HT up to the saturation point (no free rra-P3HT). (b) UV−vis absorption spectra for BNNT-rra-P3HT solutions in $CHCl_3$ at the saturation point (no free rra-P3HT) for BNNT purified at various temperatures and scattering background profiles. (c) UV−vis absorption spectra extracted from removing the scattering background profiles for BNNTs purified at various temperatures. (d) Saturation point range (S), BET surface area (S_{BET}), and quality index for the BNNTs purified at various temperatures.

purified at various temperatures. While the purity of the material increases with increasing temperature, some of the BN sheets and BN shells remained even after the highest temperature treatment. This is likely due to the etching process occurring at edges or defect sites. Crystalline surfaces react much more slowly and likely the crystalline area of the h-BN flakes react at similar or perhaps slower rates than crystalline BNNTs; thus, a large h-BN flake or shell takes much longer to eliminate than a small one. As a result, after a prescribed treatment time, small residual h-BN impurities remain. We observed that most BNNTs purified at high temperatures have clean surfaces. We hypothesize that most of the BN flakes sitting on the surface of BNNT had poor crystallinity and sizes of less than 5 nm; thus, they were more easily eliminated than larger fragments of better crystallinity and crystalline BNNTs. It is hypothesized that with longer treatment times and in combination with other reagents that all impurities can be removed from HABS-produced BNNT materials and other high temperature synthesis processes. This complete purification approach will be explored within the scope of another paper.

Chlorine is a very reactive chemical, especially at high temperatures such as those used in this work; therefore, the possibility of damaging the BNNTs through the creation of defects or surface modifications is an issue of genuine concern. To examine these possibilities in greater detail we used TEM (Figure 6 and Figure S9) and EDS (Figure S6a−d), which are more local probes than XPS and FTIR. Neither the TEM images nor the EDS results show evidence of defect sites on the BNNT surface or for the presence of functionalization. Figure 6c,d and Figure S6b,d,f show Moiré patterns typical of hexagonal bonding structures. The FFT image (insert A) of Figure 6d is also typical of hexagonal structures.[43,44]

Finally, Martinez-Rubi et al.[29] recently reported a colorimetric method to assess the relative quality of different BNNT samples which is particularly amenable to monitoring the effect of variations in synthesis and purification conditions. Quality is defined as a convolution of sample purity (i.e., fraction of nanotubes in a sample) and BNNT wall defect density. The method relies on the interaction of regiorandom poly(3-hexylthiophene) (rra-P3HT) with BNNTs and with impurities. rra-P3HT aligns on the surface of BNNTs to form a strongly bonded complex, which promotes the formation of rra-P3HT aggregates.[28] The rra-P3HT planarization and formation of aggregates induces a significant color change and leads to the emergence of structured absorption bands specific to the presence of BNNTs. No such photophysical changes occur when rra-P3HT interacts with impurities present in HABS-produced BNNT samples (e.g., h-BN and other nontubular BN derivatives).[28,29] Figure S10 shows more detail about the preparation of the samples and determination of the saturation point (S; minimum amount of rra-P3HT required to cover all

https://dx.doi.org/10.1021/acs.chemmater.0c00144
Chem. Mater. 2020, 32, 3911−3921

available BNNT surfaces for a calibrated amount of material) when a yellow/orange solution of rra-P3HT in chloroform is gradually added to BNNT samples purified at different temperatures. Once all of the available BNNT surface is covered (titrated), the intensity of the bands due to the rra-P3HT/BNNT complex ceases to grow and absorption related to free P3HT emerges.[29] Figure 7a shows the colorimetric changes at the saturation point after removal of free rra-P3HT. As the purification temperature increases, *S* increases and the solution becomes more purple indicating increasingly higher BNNT material quality. Figure 7b shows the resulting absorption spectra, and Figure 7c shows the same spectra after subtracting the scattering background (details about this process can be found in the SI). For reference, Figure S11 shows the absorption results for rra-P3HT with ap-BNNTs. Although a higher *S* value and a higher absorbance mean a higher quality BNNT material, Martinez-Rubi et al. also developed a *Quality Index* based on the absorption feature intensities to better compare samples.[29] The saturation range and quality index for each sample are shown in Figure 7d. The quality index correlates with *S* and also with the specific surface area (S_{BET}) determined from octane adsorption isotherms as shown in Figure 7d. As the purification temperature increases, more impurities, including amorphous coatings on the BNNTs and defective BNNTs, are etched away by the chlorine, leaving a higher proportion of pristine BNNTs. Therefore, for a given mass of samples, the surface available for rra-P3HT planarization and the formation of ordered aggregates increases as the quality of the material increases.

CONCLUSIONS

Molecular chlorine has been used to remove all elementary boron and to etch multiple impurity species and defective BNNTs at elevated temperatures. The approach provides a simple, fast, and effective method to purify BNNTs synthesized by high-temperature methods. Processing temperatures from 750 to 1050 °C were explored, and it was demonstrated that BNNT quality improves as the temperature is increased. The highest quality BNNTs were obtained from chlorine purification at 1050 °C, while a temperature of 950 °C offers a good compromise between purity and process yield. Although as executed here not all BN impurities have been removed, the process offers an excellent first step and a strong platform toward an entirely gas-phase process to obtain highly pure BNNTs. The main advantages of the method are (1) it is scalable, (2) it relies only on gas-phase processes, (3) it is cost-effective, and (4) it presents minimal environmental impact. Although we demonstrated scalability up to 150 g per run with our hardware, currently available commercial hardware could accommodate 600 g per run over a 4 h period. The gas-phase nature of the process makes it very attractive for industrial development by eliminating expensive solution phase processing and reducing environmental impact. It is feasible that the process shown here could be integrated with synthesis processes, such as the HABS process, to manufacture high purity BNNTs in a single closed system. This innovative and effective purification method should support the broader availability of high quality and high purity BNNTs and their adoption for diverse commercial applications.

ASSOCIATED CONTENT

Supporting Information

The Supporting Information is available free of charge at https://pubs.acs.org/doi/10.1021/acs.chemmater.0c00144.

Photograph of the purification apparatus, SEM analysis, XPS analysis, FT-IR analysis, TEM, STEM, EDS, and EELS analyses, and P3HT test of ap-BNNTs and BNNTs purified at different temperatures (PDF)

AUTHOR INFORMATION

Corresponding Author

Benoit Simard − *Security and Disruptive Technologies Research Centre, National Research Council Canada, Ottawa, Ontario K1A 0R6, Canada;* orcid.org/0000-0001-6689-4308; Email: benoit.simard@nrc-cnrc.gc.ca

Authors

Hyunjin Cho − *Security and Disruptive Technologies Research Centre, National Research Council Canada, Ottawa, Ontario K1A 0R6, Canada;* orcid.org/0000-0002-2161-4891

Steven Walker − *Security and Disruptive Technologies Research Centre, National Research Council Canada, Ottawa, Ontario K1A 0R6, Canada;* orcid.org/0000-0002-1880-7019

Mark Plunkett − *Security and Disruptive Technologies Research Centre, National Research Council Canada, Ottawa, Ontario K1A 0R6, Canada*

Dean Ruth − *Security and Disruptive Technologies Research Centre, National Research Council Canada, Ottawa, Ontario K1A 0R6, Canada*

Robyn Iannitto − *Energy, Mining and Environment Research Centre, National Research Council Canada, Ottawa, Ontario K1A 0R6, Canada;* orcid.org/0000-0003-1446-5207

Yadienka Martinez Rubi − *Security and Disruptive Technologies Research Centre, National Research Council Canada, Ottawa, Ontario K1A 0R6, Canada;* orcid.org/0000-0002-1548-6504

Keun Su Kim − *Security and Disruptive Technologies Research Centre, National Research Council Canada, Ottawa, Ontario K1A 0R6, Canada;* orcid.org/0000-0003-3358-5159

Christa M. Homenick − *Security and Disruptive Technologies Research Centre, National Research Council Canada, Ottawa, Ontario K1A 0R6, Canada;* orcid.org/0000-0002-0286-8802

Andreas Brinkmann − *Metrology Research Centre, National Research Council Canada, Ottawa, Ontario K1A 0R6, Canada;* orcid.org/0000-0001-6442-3780

Martin Couillard − *Energy, Mining and Environment Research Centre, National Research Council Canada, Ottawa, Ontario K1A 0R6, Canada*

Stéphane Dénommée − *Security and Disruptive Technologies Research Centre, National Research Council Canada, Ottawa, Ontario K1A 0R6, Canada*

Jingwen Guan − *Security and Disruptive Technologies Research Centre, National Research Council Canada, Ottawa, Ontario K1A 0R6, Canada;* orcid.org/0000-0003-1759-2172

Michael B. Jakubinek − *Security and Disruptive Technologies Research Centre, National Research Council Canada, Ottawa, Ontario K1A 0R6, Canada*

Zygmunt J. Jakubek − *Metrology Research Centre, National Research Council Canada, Ottawa, Ontario K1A 0R6, Canada;* orcid.org/0000-0003-3307-8464

https://dx.doi.org/10.1021/acs.chemmater.0c00144
Chem. Mater. 2020, 32, 3911−3921

Christopher T. Kingston − *Security and Disruptive Technologies Research Centre, National Research Council Canada, Ottawa, Ontario K1A 0R6, Canada*

Complete contact information is available at: https://pubs.acs.org/10.1021/acs.chemmater.0c00144

Author Contributions

The manuscript was written through contributions of all authors. All authors have given approval to the final version of the manuscript.

Notes

The authors declare no competing financial interest.

■ ACKNOWLEDGMENTS

This work was supported by the NRC through its Security Materials Technology Program. H.C. acknowledges the AFOSR (FA9550-18-1-0014) for the financial support. The authors are grateful to Malgosia Daroszewska for the DVS and TGA measurements and to Oltion Kodra for XPS measurements.

■ REFERENCES

(1) Chopra, N. G.; Luyken, R.; Cherrey, K.; Crespi, V. H.; Cohen, M. L.; Louie, S. G.; Zettl, A. Boron nitride nanotubes. *Science* **1995**, *269* (5226), 966−967.

(2) Loiseau, A.; Willaime, F.; Demoncy, N.; Schramchenko, N.; Hug, G.; Colliex, C.; Pascard, H. Boron nitride nanotubes. *Carbon* **1998**, *36* (5−6), 743−752.

(3) Terauchi, M.; Tanaka, M.; Matsumoto, T.; Saito, Y. Electron energy-loss spectroscopy study of the electronic structure of boron nitride nanotubes. *J. Electron Microsc.* **1998**, *47* (4), 319−324.

(4) Golberg, D.; Bando, Y.; Tang, C.; Zhi, C. Boron nitride nanotubes. *Adv. Mater.* **2007**, *19* (18), 2413−2432.

(5) Zhi, C.; Bando, Y.; Tang, C.; Huang, Q.; Golberg, D. Boron nitride nanotubes: functionalization and composites. *J. Mater. Chem.* **2008**, *18* (33), 3900−3908.

(6) Zhi, C.; Bando, Y.; Tang, C.; Golberg, D. Boron nitride nanotubes. *Mater. Sci. Eng., R* **2010**, *70* (3−6), 92−111.

(7) Cohen, M. L.; Zettl, A. The physics of boron nitride nanotubes. *Phys. Today* **2010**, *63* (11), 34−38.

(8) Golberg, D.; Bando, Y.; Huang, Y.; Terao, T.; Mitome, M.; Tang, C.; Zhi, C. Boron nitride nanotubes and nanosheets. *ACS Nano* **2010**, *4* (6), 2979−2993.

(9) Wang, J.; Lee, C. H.; Yap, Y. K. Recent advancements in boron nitride nanotubes. *Nanoscale* **2010**, *2* (10), 2028−2034.

(10) Thibeault, S. A.; Kang, J. H.; Sauti, G.; Park, C.; Fay, C. C.; King, G. C. Nanomaterials for radiation shielding. *MRS Bull.* **2015**, *40* (10), 836−841.

(11) Kim, J. H.; Pham, T. V.; Hwang, J. H.; Kim, C. S.; Kim, M. J. Boron nitride nanotubes: synthesis and applications. *Nano Converg.* **2018**, *5* (1), 17.

(12) Kim, K. S.; Kim, M. J.; Park, C.; Fay, C. C.; Chu, S.-H.; Kingston, C. T.; Simard, B. Scalable manufacturing of boron nitride nanotubes and their assemblies: a review. *Semicond. Sci. Technol.* **2017**, *32* (1), 013003.

(13) Jakubinek, M. B.; Ashrafi, B.; Martinez-Rubi, Y.; Guan, J.; Rahmat, M.; Kim, K. S.; Dénommée, S.; Kingston, C. T.; Simard, B. Boron Nitride Nanotube Composites and Applications. In *Nanotube Superfiber Materials*, 2nd ed.; Schulz, M. J., Shanov, V., Yin, Z., Cahay, M., Eds.; William Andrew Publishing: Norwich, NY, U.S.A., 2019; Chapter 5, pp 91−111.

(14) Huang, Y.; Lin, J.; Tang, C.; Bando, Y.; Zhi, C.; Zhai, T.; Dierre, B.; Sekiguchi, T.; Golberg, D. Bulk synthesis, growth mechanism and properties of highly pure ultrafine boron nitride nanotubes with diameters of sub-10 nm. *Nanotechnology* **2011**, *22* (14), 145602.

(15) E, S.; Wu, L.; Li, C.; Zhu, Z.; Long, X.; Geng, R.; Zhang, J.; Li, Z.; Lu, W.; Yao, Y. Growth of boron nitride nanotubes from magnesium diboride catalysts. *Nanoscale* **2018**, *10* (29), 13895−13901.

(16) Smith, M. W.; Jordan, K. C.; Park, C.; Kim, J.-W.; Lillehei, P. T.; Crooks, R.; Harrison, J. S. Very long single-and few-walled boron nitride nanotubes via the pressurized vapor/condenser method. *Nanotechnology* **2009**, *20* (50), 505604.

(17) Kim, K. S.; Kingston, C. T.; Hrdina, A.; Jakubinek, M. B.; Guan, J.; Plunkett, M.; Simard, B. Hydrogen-catalyzed, pilot-scale production of small-diameter boron nitride nanotubes and their macroscopic assemblies. *ACS Nano* **2014**, *8* (6), 6211−6220.

(18) Kim, K. S.; Couillard, M.; Shin, H.; Plunkett, M.; Ruth, D.; Kingston, C. T.; Simard, B. Role of Hydrogen in High-Yield Growth of Boron Nitride Nanotubes at Atmospheric Pressure by Induction Thermal Plasma. *ACS Nano* **2018**, *12* (1), 884−893.

(19) Fathalizadeh, A.; Pham, T.; Mickelson, W.; Zettl, A. Scaled synthesis of boron nitride nanotubes, nanoribbons, and nanococoons using direct feedstock injection into an extended-pressure, inductively-coupled thermal plasma. *Nano Lett.* **2014**, *14* (8), 4881−4886.

(20) Kim, J. H.; Cho, H.; Pham, T. V.; Hwang, J. H.; Ahn, S.; Jang, S. G.; Lee, H.; Park, C.; Kim, C. S.; Kim, M. J. Dual growth mode of boron nitride nanotubes in high temperature pressure laser ablation. *Sci. Rep.* **2019**, *9* (1), 15674.

(21) Chen, H.; Chen, Y.; Yu, J.; Williams, J. S. Purification of boron nitride nanotubes. *Chem. Phys. Lett.* **2006**, *425* (4−6), 315−319.

(22) Guan, J.; Kim, K. S.; Jakubinek, M. B.; Simard, B. pH-Switchable Water-Soluble Boron Nitride Nanotubes. *ChemistrySelect* **2018**, *3* (32), 9308−9312.

(23) Kleinerman, O.; Adnan, M.; Marincel, D. M.; Ma, A. W.; Bengio, E. A.; Park, C.; Chu, S.-H.; Pasquali, M.; Talmon, Y. Dissolution and Characterization of Boron Nitride Nanotubes in Superacid. *Langmuir* **2017**, *33* (50), 14340−14346.

(24) Amin, M. S.; Atwater, B.; Pike, R. D.; Williamson, K. E.; Kranbuehl, D. E.; Schniepp, H. C. High-Purity Boron Nitride Nanotubes via High-Yield Hydrocarbon Solvent Processing. *Chem. Mater.* **2019**, *31* (20), 8351−8357.

(25) Marincel, D.; Adnan, M.; Ma, J.; Bengio, E. A.; Trafford, M.; Kleinerman, O.; Kosynkin, D. V.; Chu, S.-H.; Park, C.; Hocker, S. J.; et al. Scalable Purification of Boron Nitride Nanotubes via Wet Thermal Etching. *Chem. Mater.* **2019**, *31* (5), 1520−1527.

(26) Al-Antaki, A. H. M.; Lawrance, W. D.; Raston, C. L. Dynamic thin film mediated slicing of boron nitride nanotubes. *Nanoscale Adv.* **2019**, *1*, 4722−4728.

(27) Hung, C.-C.; Hurst, J. Purifying Nanomaterials. US 8734748B1, 2014.

(28) Martinez-Rubi, Y.; Jakubek, Z. J.; Jakubinek, M. B.; Kim, K. S.; Cheng, F.; Couillard, M.; Kingston, C.; Simard, B. Self-assembly and visualization of poly (3-hexyl-thiophene) chain alignment along boron nitride nanotubes. *J. Phys. Chem. C* **2015**, *119* (47), 26605−26610.

(29) Martinez Rubi, Y.; Jakubek, Z. J.; Chen, M.; Zou, S.; Simard, B. Quality Assessment of Bulk Boron Nitride Nanotubes for Advancing Research, Commercial, and Industrial Applications. *ACS Appl. Nano Mater.* **2019**, *2* (4), 2054−2063.

(30) Bernard, S.; Miele, P. Nanostructured and architectured boron nitride from boron, nitrogen and hydrogen-containing molecular and polymeric precursors. *Mater. Today* **2014**, *17* (9), 443−450.

(31) Bartl, A.; Bohr, S.; Haubner, R.; Lux, B. A comparison of low-pressure CVD synthesis of diamond and c-BN. *Int. J. Refract. Hard Met.* **1996**, *14* (1−3), 145−157.

(32) Jakubinek, M. B.; Kim, K. S.; Homenick, C.; Kodra, O.; Walker, S.; Simard, B. Assessment of boron nitride nanotube materials using X-ray photoelectron spectroscopy. *Can. J. Chem.* **2019**, *97* (6), 457−464.

(33) Kentgens, A. A practical guide to solid-state NMR of half-integer quadrupolar nuclei with some applications to disordered systems. *Geoderma* **1997**, *80* (3−4), 271−306.

(34) Jeschke, G.; Hoffbauer, W.; Jansen, M. A comprehensive NMR study of cubic and hexagonal boron nitride. *Solid State Nucl. Magn. Reson.* **1998**, *12* (1), 1−7.
(35) Love, A. M.; Thomas, B.; Specht, S. E.; Hanrahan, M. P.; Venegas, J. M.; Burt, S. P.; Grant, J. T.; Cendejas, M. C.; McDermott, W. P.; Rossini, A. J.; et al. Probing the Transformation of Boron Nitride Catalysts under Oxidative Dehydrogenation Conditions. *J. Am. Chem. Soc.* **2019**, *141* (1), 182−190.
(36) Panich, A.; Shames, A.; Froumin, N.; Tang, C.; Bando, Y. Magnetic resonance study of multiwall boron nitride nanotubes. *Phys. Rev. B: Condens. Matter Mater. Phys.* **2005**, *72* (8), 085307.
(37) Turner, C. L.; Taylor, R.; Kaner, R. B. 10B and 11B NMR study of elemental boron. *J. Phys. Chem. C* **2015**, *119* (24), 13807−13813.
(38) Jung, J. K.; Ryu, K.-S.; Kim, Y.-I.; Tang, C. NMR study of boron nitride nanotubes. *Solid State Commun.* **2004**, *130* (1−2), 45−48.
(39) Kim, Y.-I.; Jung, J. K.; Ryu, K.-S.; Nahm, S.-H.; Gregory, D. H. Quantitative phase analysis of boron nitride nanotubes using Rietveld refinement. *J. Phys. D: Appl. Phys.* **2005**, *38* (8), 1127.
(40) Wu, J.; Potuzak, M.; Stebbins, J. F. High-temperature in situ11B NMR study of network dynamics in boron-containing glass-forming liquids. *J. Non-Cryst. Solids* **2011**, *357* (24), 3944−3951.
(41) Sen, S.; Xu, Z.; Stebbins, J. Temperature dependent structural changes in borate, borosilicate and boroaluminate liquids: high-resolution 11B, 29Si and 27Al NMR studies. *J. Non-Cryst. Solids* **1998**, *226* (1−2), 29−40.
(42) Harrison, H.; Lamb, J. T.; Nowlin, K. S.; Guenthner, A. J.; Ghiassi, K. B.; Kelkar, A. D.; Alston, J. R. Quantification of hexagonal boron nitride impurities in boron nitride nanotubes via FTIR spectroscopy. *Nanoscale Adv.* **2019**, *1*, 1693−1701.
(43) Joucken, F.; Frising, F.; Sporken, R. Fourier transform analysis of STM images of multilayer graphene moiré patterns. *Carbon* **2015**, *83*, 48−52.
(44) Stępniowski, W. J.; Michalska-Domańska, M.; Norek, M.; Czujko, T. Fast Fourier transform based arrangement analysis of poorly organized alumina nanopores formed via self-organized anodization in chromic acid. *Mater. Lett.* **2014**, *117*, 69−73.

https://dx.doi.org/10.1021/acs.chemmater.0c00144
Chem. Mater. 2020, 32, 3911−3921